
超低損失ベアリングレスグラファイトモータの原理解明と実機検証

Principle and Experimental Validation in Ultralow Loss Bearingless Graphite Motor

M22助自42

代表研究者 杉 元 紘 也 東京電機大学 工学部 電気電子工学科 准教授
Hiroya Sugimoto Associate Professor, Department of Electrical and Electronic Engineering,
Tokyo Denki University

Toward carbon neutrality, increasing motor efficiency has been strongly required for energy-saving in industry applications. One of the possible solutions is bearingless motor technologies because mechanical bearing losses can be removed. Bearingless motors also have other notable benefits of long life-time and maintenance-free because of non-contact without mechanical bearings. This article proposes a novel rotor design of diamagnetic bearingless motors. Generally, one or more degrees of freedom should be actively regulated to stabilize the rotor shaft with magnetic suspensions. In contrast, fully passively stabilized bearingless motors have several advantages of eliminating displacement sensors, inverters, and magnetic suspension powers. In these machines, five degrees of freedom are passively stabilized and only rotation is actively controlled. The rotor material is pyrolytic graphite (PG) so that five degrees of freedom of the rotor are passively stabilized above a permanent magnet array. The stator consists of two components of a Halbach permanent magnet array and an axial-flux stator core with twelve teeth holding the eight-pole three-phase winding. Passive levitation forces are generated between the permanent magnet unit and the PG rotor. However, these stiffness are low compared to typical passive magnetic bearings, in particular, the radial stiffness is seriously low. In this article, a new rotor design is proposed to improve the radial stiffness, and the proposed PG rotor is fabricated and tested. In experiments, it is demonstrated that the radial stiffness is increased by 2.45 times. In addition, the proposed rotor can improve maximum rotational speed by 43% because a critical speed is changed to high-speed region.

研究目的

In this article, a novel rotor design is proposed to improve the radial stiffness. The proposed PG rotor is not salient-pole structure but cylindrical shape with several holes. The design concept and the principle for increasing the radial stiffness are explained. In experiments, three passive stiffness of axial, tilting and radial directions are measured and compared to that of the previous salient-pole

PG rotor. It is verified that the radial stiffness is improved by 2.45 times and the rotational speed can be increased up to 286 r/min.

概要

Toward carbon neutrality, increasing motor efficiency has been strongly required for energy-saving in industry applications. One of the possible solutions is bearingless motor technologies because mechanical bearing losses can be removed.

Bearingless motors also have other notable benefits of long life-time and maintenance-free because of non-contact without mechanical bearings. Therefore, bearingless motors have been studied in a lot of applications, including centrifugal pumps for semiconductor manufacturing and artificial hearts, stirring devices, rotating stages, flywheels, compressors, and cooling fans.

Generally, one or more degrees of freedom should be actively regulated to stabilize the rotor shaft with magnetic suspensions. In contrast, fully passively stabilized bearingless motors have several advantages of eliminating displacement sensors, inverters, and magnetic suspension powers. In these machines, five degrees of freedom are passively stabilized and only rotation is actively controlled. In several papers, electrodynamic forces are employed for passive stabilization. It also requires touch-down bearings or active magnetic suspensions at low-speed region. In other papers, diamagnetic graphite materials have been used, and it can achieve the static magnetic levitation. In our previous studies, we have proposed a unique concept of pyrolytic graphite (PG) bearingless motor as shown in Fig. 1. The previous machine has a salient-pole PG rotor, and it is successfully levitated and rotated up to 200 r/min. On the other hand, the rotational speed is limited due to a critical speed that is caused by radial stiffness.

In literature review regarding measurement of passive radial stiffness, the radial stiffness of six square PG sheets are measured. Although their stiffness are approximately $7 \mu\text{N}/\text{mm} \sim 30 \mu\text{N}/\text{mm}$, the highest natural frequency is 9.55 Hz because the mass of the PG sheet is approximately

0.003 g. It is experimentally confirmed that the weight reduction of the PG sheet contributes to increase the natural frequency. In other one, magnetic potential energies of PG disks with and without a center hole are compared when the disk is displaced in the radial direction. The annular PG disk has large difference of the magnetic potential energy, and it means that it has high passive radial stiffness.

In this article, a novel rotor design is proposed to improve the radial stiffness. The proposed PG rotor is not salient-pole structure but cylindrical shape with several holes. The design concept and the principle for increasing the radial stiffness are explained. In experiments, three passive stiffness of axial, tilting and radial directions are measured and compared to that of the previous salient-pole PG rotor. It is verified that the radial stiffness is improved from 2.92 mNm/mm to 7.16 mN/mm. It is 2.45 times, and it is experimentally demonstrated that the slitted PG rotor can enhance the passive radial stiffness. Furthermore, the proposed rotor can increase the rotational speed up to 286 r/min. These achievements have been presented in domestic and international academic conferences in IEEJ and IEEE. In future works, the slitted rotor design will be improved to enhance the radial stiffness. In addition, the rotating torque will be increased by improved axial-flux stator. These improvements will contribute to increase rotational speed of bearingless graphite motors.

本 文

Figure 1 shows a bearingless graphite motor which five degrees of freedom are passively stabilized. The rotor is a diamagnetic pyrolytic graphite (PG) plate with salient poles so that it is passively

levitated above permanent magnets. A Halbach array is applied to enhance air-gap flux density in the permanent magnet. An axial-flux stator core is installed above the PG rotor to generate rotating torque using electromagnetic forces. In the previous study, the PG rotor was accelerated up to 200 r/min with the complete passive magnetic suspension. When the rotational speed was increased around 210 r/min, the rotor radial vibration was extremely increased due to the resonant frequency. As a result, the PG rotor was thrown out of the stator in the radial direction. In this article, the passive radial stiffness is improved to move the resonance to higher frequency. Let us define coordinates of radial, circumference and axial directions as r , ϕ_s and z , respectively.

Figure 2(a) shows a flux density distribution around the diamagnetic PG rotor above the Halbach array permanent magnet. This figure assumes the right half plane of Fig. 1 without the upper stator. Here the flux density B is approximately expressed as sinusoidal waveform with the amplitude B_m .

$$B = B_m \cos 2\theta \dots \dots \dots (1)$$

The energy W_m of the diamagnetic PG rotor with volume is expressed with square of the flux density, permeability μ_0 and magnetic susceptibility c_m .

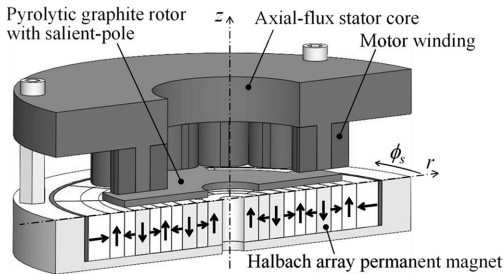


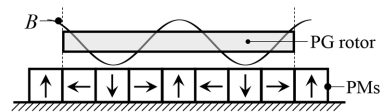
Fig. 1 Bearingless graphite motor with a salient-pole diamagnetic rotor.

$$W_m = \int_V \frac{\chi_m B^2}{2\mu_0} dV \dots \dots \dots (2)$$

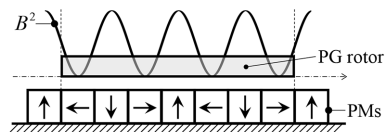
Figure 2(b) shows the waveform of the square of flux density when the diamagnetic PG rotor is centered. On the other hand, Figure 2(c) shows changed energies at the rotor radial displacement of Δr . Hatched areas of W_1 and W_2 are increased and decreased energies, respectively. The passive radial force F_r is given as follows with a differential of the energy with respect to the radial displacement.

$$F_r = \frac{W_1 - W_2}{\Delta r} = \frac{\chi_m}{2\mu_0} \int_V \frac{\partial B^2}{\partial r} dV \dots \dots \dots (3)$$

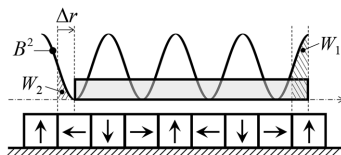
In case of pyrolytic graphite materials, the susceptibility is -450×10^{-6} , and the negative coefficient results in generating passive radial forces. Figure 3(a) shows a slitted PG rotor that has a slit at center of the rotor. Let us suppose that their left and right parts are integrated. Figure 3(b) shows the energy variation in the case of the slitted PG rotor with radial displacement. The changed



(a) Waveform of flux density around levitated PG rotor.



(b) Waveform of square of flux density around levitated PG rotor.



(c) Differential of energy of PG rotor at radial displacement.

Fig. 2 Principle of passive radial force generation in previous PG rotor without holes.

area of the energy is double because it is created around the slit in addition to both sides of the rotor. Therefore, the passive radial force of the slitted rotor F_r' is double compared to the previous solid rotor.

$$F_r' = \frac{2(W_1 - W_2)}{\Delta r} = 2F_r \dots \dots \dots (4)$$

In order to increase the passive radial force, slits should be placed above a permanent magnet that is magnetized in the axial direction. In contrast, the passive axial force is decreased because diamagnetic material is removed where high axial force is generated. Therefore, the slit should be carefully placed in the diamagnetic PG rotor.

Figure 4 shows top and cut views of the proposed slitted PG rotor. The outer diameter and the thickness are 60 mm and 1.5 mm, respectively. It is passively levitated above the permanent magnet array, and magnetization directions are indicated by arrows in the cut view. The proposed PG rotor has several holes that are made just above permanent magnets magnetized in axial direction. The hole is a significant key to enhance the radial stiffness as well as reducing rotor weight.

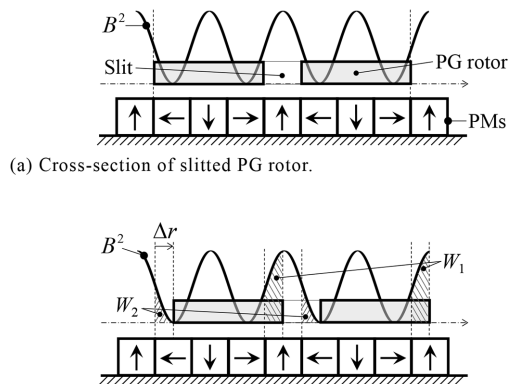


Fig. 3 Design concept of proposed PG rotor with holes for improvement of passive radial stiffness.

Figure 5 shows calculated square of flux density in air region above the permanent magnet array. Holes are created just above permanent magnets that are magnetized in the axial direction. In Fig. 3, holes in the PG rotor are located at high rate of change of the flux density, and the passive radial force is generated around edges of their holes.

Figures 6(a) and 6(b) show fabricated two rotors. The previous structure has five salient poles, and similar rotor structure with four salient poles is already proposed. Fig. 6(b) shows the proposed slitted PG rotor. The outer circumference of the rotor has bridges to connect in between salient

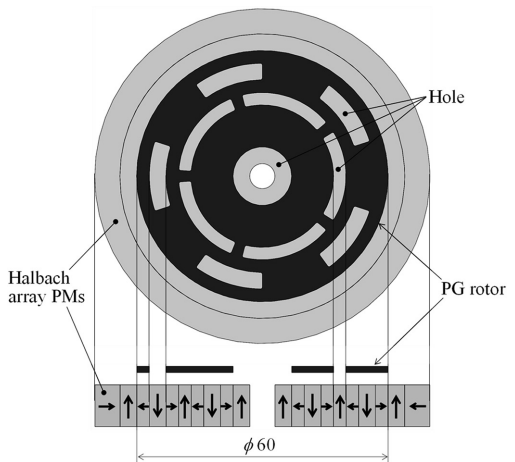


Fig. 4 Proposed slitted PG rotor.

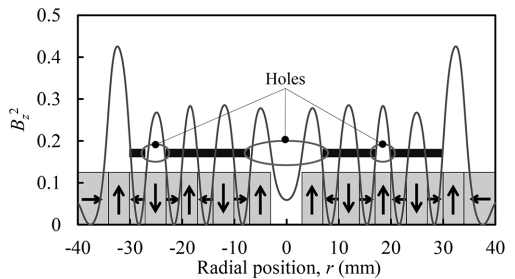


Fig. 5 Calculated square of flux density above the Halbach array permanent magnet. Holes are created just above permanent magnets that are magnetized in axial direction.

poles so that it is a cylindrical rotor. Table I shows designed parameters of two rotors. These rotor masses are 6.88 g and 6.80 g, respectively, in the previous and proposed rotors; and therefore, they are mostly identical in the two rotors. On the other hand, an inertia around the rotational axis is increased from $2.86 \times 10^{-6} \text{ kg}\cdot\text{m}^2$ to $3.24 \times 10^{-6} \text{ kg}\cdot\text{m}^2$ because the mass distribution is changed to outside due to making slits and outer bridges.

Figures 7(a) and 7(b) show side views of levitated previous and proposed PG rotors. Both these rotors are passively levitated at the center position. Their levitation heights are mostly the identical; and therefore, it is confirmed that the

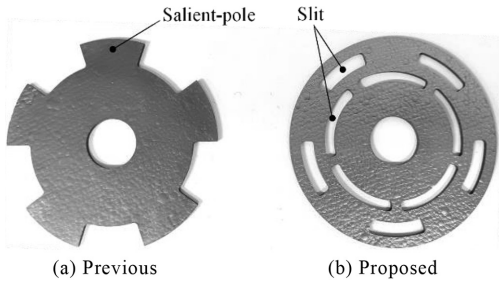


Fig. 6 Fabricated rotors of (a) previous structure with five salient poles and (b) proposed slitted structure.



(a) Previous salient-pole rotor (b) Proposed slitted PG rotor
Fig. 7 Side views of levitated PG rotors above Halbach array permanent magnet.

TABLE I DESIGNED PARAMETERS OF PREVIOUS AND PROPOSED ROTORS

Parameter	Previous rotor with salient-pole	Proposed rotor with flux barrier	Unit
Outer diameter of PG rotor	60	60	mm
Axial length of PG rotor	1.5	1.5	mm
Number of rotor poles	5	5	
Rotor mass, m	6.88	6.80	g
Inertia around x- and y-axis	1.43×10^{-6}	1.62×10^{-6}	$\text{kg}\cdot\text{m}^2$
Inertia around rotational axis	2.86×10^{-6}	3.24×10^{-6}	$\text{kg}\cdot\text{m}^2$

slitted PG rotor can generate sufficient axial force to suspend the rotor weight even when several partials of the rotor are hollowed.

Figure 8 shows the fabricated axial-flux stator with twelve slots. It has three-phase concentrated windings with ten poles because those PG rotors look like ten-pole homopolar rotor structure that is created by bias fluxes from the stator permanent magnet. The rotating torque is generated around salient poles in the previous rotor because electromagnetic forces are generated by superimposing winding fluxes on the bias flux. Note that it is not attractive but repulsive forces because of negative magnetic susceptibility, and as a result, the repulsive torque is generated in the PG rotor. This principle can be applied to the slitted PG rotor because only bridges are added between salient poles. In fact, the stator tooth width in the radial direction is aligned to the slit width of 4 mm in the slitted rotor. The number of series turns is 168 per phase. The rated rms current is 2 A.

Figure 9 shows measurement system of passive radial stiffness. It can be measured from the natural frequency, and it is obtained in the waveform of free vibration when an impulse disturbance is applied. Let us define the rotor mass, natural



Fig. 8 Fabricated axial-flux stator.

frequency, and radial stiffness as m, f_{nr} , and k_r .

Then, radial stiffness can be expressed as follows:

$$k_r = m (2\pi f_{nr})^2 \dots \dots \dots (5)$$

Similarly, the axial and tilting stiffness can be calculated with their natural frequencies f_{nz} and f_{nq} .

Let us define these stiffness and inertia around x - and y -axis as k_z, k_q and J_r . Their stiffness are given as follows:

$$k_z = m (2\pi f_{nz})^2 \dots \dots \dots (6)$$

$$k_\theta = J_r (2\pi f_{n\theta})^2 \dots \dots \dots (7)$$

The radial vibration waveform is measured by a laser sensor that is installed in the horizontal direction as shown in Figure 9. The sensor target is a side surface of the proposed PG rotor with thickness of 1.5 mm as shown in Fig. 9(a). In the case of the previous PG rotor, the side surface of salient-pole is used for the sensor target as shown in Fig. 9(b).

Figures 10(a) and 10(b) show measured radial vibration waveforms in the previous and proposed PG rotors when the impulse disturbance is applied to radial direction. These measured natural frequencies are 3.28 Hz and 5.17 Hz, respectively. Their radial stiffness can be calculated by (5), and they are 2.92 mN/mm and 7.16 mN/mm, respectively. Therefore, it is experimentally demonstrated that the proposed slitted PG rotor can improve passive radial stiffness by 2.45 times. In addition, the radial vibration is converged due to eddy currents and air frictions so that the PG rotor has damping effects. While the PG rotor is

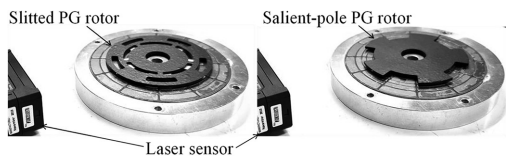
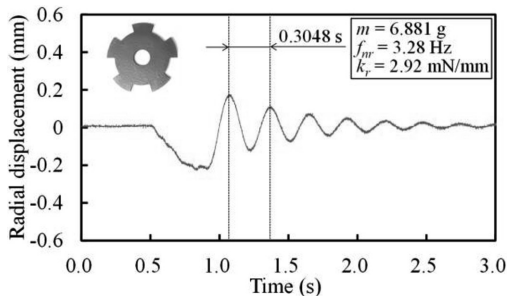


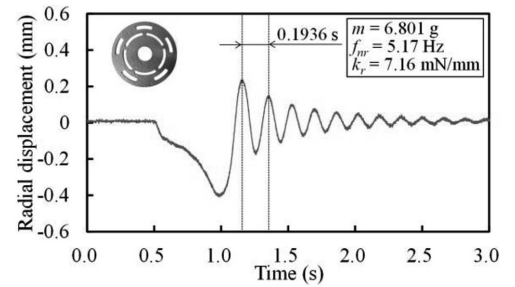
Fig. 9 Measurement systems of passive radial stiffness.

rotating at the center position, the eddy current loss is quite low because the flux density is constant in the circumference direction. In contrast, the flux density is changed when the PG rotor is moved in the radial direction as shown in Fig. 3. It generates both the passive radial force and the damping force. Therefore, the ring-shaped Halbach array permanent magnet is significantly reasonable for the bearingless graphite motor.

Figure 11 shows measured passive axial forces



(a) Previous rotor with five salient poles



(b) Proposed cylindrical rotor with holes

Fig. 10 Measured vibration waveforms of levitated two rotors at impulse response.

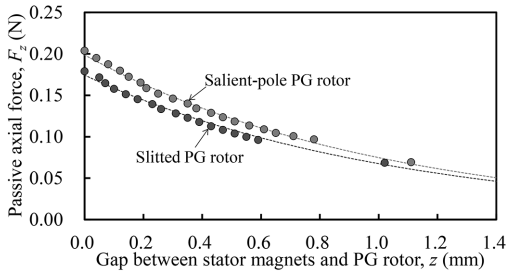


Fig. 11 Measured passive axial force with respect to axial displacement in previous and proposed rotors.

with respect to air-gap between the stator magnet and the levitated PG rotor. Nineteen aluminum plates which have different outer diameters are put on the levitated PG rotor one by one as an axial load. Then, the passive axial force is calculated from sum of weights of the aluminum plate and the PG rotor. The air-gap length is decreased with an increase of the load, and maximum passive axial forces are 0.203 N and 0.187 N, respectively, in the previous salient-pole and proposed slitted PG rotors. Although it is slightly decreased due to the slit, the passive axial force is high enough against the rotor weight.

Table II shows measured passive stiffness in the radial, axial and tilting directions in the previous and proposed PG rotors. The axial and tilting stiffness are also measured in impulse disturbance tests. The axial stiffness is slightly decreased from 66.3 mN/mm to 60.1 mN/mm in the proposed rotor. The tilting stiffness of the slitted rotor is mostly identical to the salient-pole rotor, and it is 16.2 mNm/rad. Therefore, the advantage of the proposed slitted rotor is enhancement of the radial stiffness by 2.45 times with keeping identical axial

and tilting stiffness. Calculated critical speeds of radial, axial and tilting directions are 196 r/min, 924 r/min and 948 r/min, respectively, in the previous salient-pole rotor. In the case of the proposed slitted rotor, they are 311 r/min, 882 r/min and 954 r/min, respectively; and therefore, the critical speed of the radial direction can be increased by approximately 1.6 times. It can be expected to improve the rotational speed by increasing the critical speed.

Figure 12 shows the assembled prototype machine with 12-slot axial flux stator. The stator has 10-pole three-phase winding. The air-gap length is 4 mm between upper surface of the Halbach array permanent magnet and the stator tooth tip. The proposed PG rotor is passively levitated between lower and upper stators. The radial and tilting motions are also passively stabilized. The radial vibration is measured by the laser sensor, and the rotational speed is measured by a tachometer. Since five sensor target marks are attached on the PG rotor, indicated speed is five times of the actual one. Therefore, it is 265 r/min when the indicated value is 1327 as shown in Fig. 12. In the drive system, the DC link voltage and the

TABLE II MEASURED PASSIVE STIFFNESS AND CRITICAL SPEED

Parameter	Previous rotor with salient-pole	Proposed rotor with flux barrier	Unit
Measured natural frequency in radial direction, f_{nr}	3.28	5.17	Hz
Measured natural frequency in axial direction, f_{nz}	15.4	14.7	Hz
Measured natural frequency in tilting direction, f_{nt}	15.8	15.9	Hz
Passive radial stiffness, k_r	2.92	7.16	mN/mm
Passive axial stiffness, k_z	66.3	60.1	mN/mm
Passive tilting stiffness, k_θ	14.2	16.2	mNm/rad
Critical speed in radial direction	196	311	r/min
Critical speed in axial direction	924	882	r/min
Critical speed in tilting direction	948	954	r/min

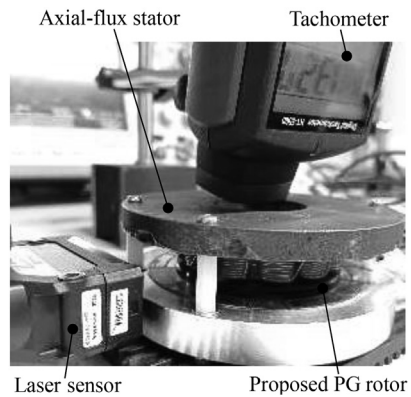


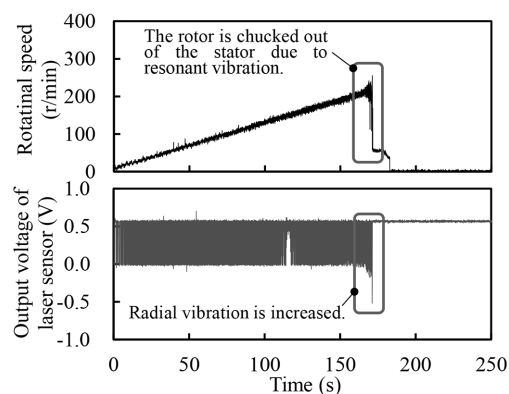
Fig. 12 Assembled prototype machine with 12-slot axial-flux stator.

phase current are 24 V and 4 Arms, respectively.

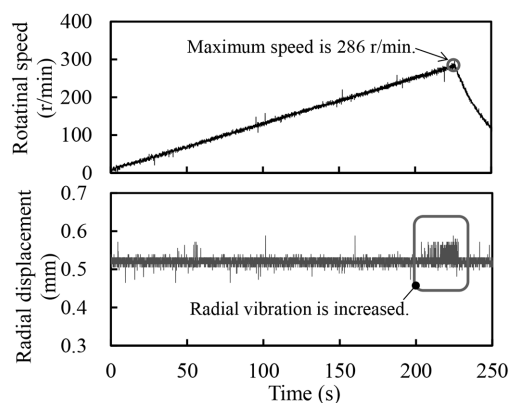
Figures 13(a) and 13(b) show measured acceleration waveforms in the previous and proposed PG rotors. In Fig. 13(a), the rotor radial vibration is increased at around 200 r/min, and then, the previous rotor is thrown out of the stator. This radial vibration is caused by the resonance of the radial stiffness. In fact, the critical speed is 196 r/min in Table II. The output voltage of the laser sensor in the previous PG rotor seems like vibrations during acceleration because the sensor is detecting salient poles and hollowed portions. The actual vibration can be identified when the output

voltage is increased compared to the constant vibration. The previous rotor can not overcome the critical speed due to the serious radial vibration. In contrast, the proposed rotor can increase the rotational speed up to 286 r/min as shown in Fig. 13(b). The radial vibration does not occur around 200 r/min, and it would be around 311 r/min. Therefore, it is verified that the proposed slitted PG rotor is effective to enhance the passive radial stiffness and improve rotational speed. In these acceleration tests, the maximum rotational speed can be improved from 200 r/min to 286 r/min, and the proposed slitted PG rotor has a potential to increase the rotational speed over 300 r/min.

This article presents the novel design of pyrolytic graphite rotor to improve the radial stiffness. The principle that the radial stiffness can be increased with slitted rotor is explained. The proposed slitted PG rotor can improve the radial stiffness by 2.45 times compared to the previous salient-pole PG rotor. In addition, the rotational speed can be increased by 43% because the critical speed in the radial direction is improved by 1.6 times.



(a) Previous salient-pole PG rotor



(b) Proposed slitted PG rotor

Fig. 13 Measured acceleration waveform of rotational speed in proposed five-axis passively stabilized bearingless motor.

今後の研究の見通し

本研究において、反磁性体グラファイト回転子に効果的に穴を空けることで、パッシブな半径方向の剛性が2.45倍に向上することが明らかになり、危険速度を196 r/minから311 r/minに増加させることができたため、結果的に最高回転速度を200 r/minから286 r/minまで向上することができた。一方、提案形状のスリット付き回転子は、危険速度に到達する前に脱調してしまっており、トルク不足の課題が明確になった。現在、アキシアルフラックス形固定子の改良を行っており、巻数を増やし350 r/minに到達している状況である。これまでのベ

アリングレスグラファイトモータの最高回転速度は、スイスのEPFLが開発した静電モータ式の300r/minであったが、本研究によりベアリングレスグラファイトモータの世界最高回転速度を更新した。今後、さらに回転子と固定子の形状を改良し、トルクを向上することで回転速度向上を目指し、ベアリングレスグラファイトモータの学術的価値を高める研究を行う予定である。

本助成金による主な発表論文、著書名

- 1) 目木祥太郎, 杉元紘也:「スリット付き反磁性体回転子による5軸受動安定形ベアリングレスグラファイトモータの半径方向剛性の向上」, 2023年電気学会産業応用部門大会講演論文集, Y-128, 2023.
- 2) Hiroya Sugimoto, and Shotaro Meki, “Rotor Designs in Pyrolytic Graphite Bearingless Motor for Increased Passive Radial Stiffness,” in *Proc., IEEE Energy Conversion Congress and Expo (ECCE2023)*, Oct., 2023. (11/1 (水)の“Bearingless and High-Speed Machines”のオーラルセッションで口頭発表予定, <https://www.ieee-ecce.org/2023/>)